

# Efficacious symmetry-adapted atomic displacement method for lattice dynamical studies

Chee Kwan Gan\*

*Institute of High Performance Computing, 1 Fusionopolis Way, #16-16 Conneris 138632, Singapore*

Yun Liu

*Cavendish Laboratory, University of Cambridge, 19 JJ Thomson Avenue, Cambridge CB3 0HE, United Kingdom*

Tze Chien Sum

*Division of Physics and Applied Physics, School of Physical and Mathematical Sciences,  
Nanyang Technological University, 21 Nanyang Link 637371, Singapore*

Kedar Hippalgaonkar

*Institute of Materials Research and Engineering (IMRE),  
A\*STAR Agency for Science, Technology and Research,  
2 Fusionopolis Way, #08-03 Innovis 138634, Singapore and  
School of Materials Science and Engineering, Nanyang Technological University, 639798, Singapore  
(Dated: Sep 17, 2020)*

Small displacement methods have been successfully used to calculate the lattice dynamical properties of crystals. It involves displacing atoms by a small amount in order to calculate the induced forces on all atoms in a supercell for the computation of force constants. Even though these methods are widely in use, to our knowledge, there is no systematic discussion of optimal displacement directions from the crystal's symmetry point of view nor a rigorous error analysis of such methods. Based on the group theory and point group symmetry of a crystal, we propose displacement directions, with an equivalent concept of the group of  $k$ , deduced directly in the Cartesian coordinates rather than the usual fractional coordinates, that maintain the theoretical maximum for the triple product  $V$  spanned by the three displacements to avoid possible severe roundoff errors. The proposed displacement directions are generated from a minimal set of irreducible atomic displacements that keep the required independent force calculations to a minimum. We find the error in the calculated force constants explicitly depends on the inverse of  $V$  and inaccuracy of the forces. Test systems such as Si, graphene, and orthorhombic  $\text{Sb}_2\text{S}_3$  are used to illustrate the method. Our symmetry-adapted atomic displacement method is shown to be very robust in treating low-symmetry cells with a large 'aspect ratio' due to huge differences in lattice parameters, use of a large vacuum height, or a very oblique unit cell due to unconventional choice of primitive lattice vectors. It is expected that our atomic displacement strategy can be used to address higher-order interatomic interactions to achieve good accuracy and efficiency.

Keywords: Phonons, Symmetries, Lattice dynamics, Group theory

## I. INTRODUCTION

Lattice dynamical studies[1] are important for an understanding of the phase stability,[2, 3] ferroelectric transition,[4] Raman and infra-red spectroscopies,[5–7] phonon-mediated superconductivity,[8] ferroelastic transition,[9] and thermodynamics of materials.[10, 11] Even though the concept of phonon emerges as a result of a harmonic approximation, its simple extensions via the quasiharmonic approximation (QHA)[12] and Grüneisen formalism[13, 14] allow thermal properties due to anharmonic effects such as lattice thermal conductivities[15], a key quantity that determine the figure of merits for thermoelectrics[16–18], as well as thermal expansion coefficients[19–24] to be evaluated. An attempt has been made to extract the third order interatomic force con-

stants from the standard phonon calculations through the evaluation of Grüneisen parameters[25]. Phonon databases are being built[26, 27] with the help of high-throughput frameworks[28–30] for data mining and machine learning.

The methods to calculate phonon frequencies and eigenvectors naturally fall into two distinct approaches. One approach is based on the displacement methods[3, 31–38] that gain popularity due to their simplicity in implementations. In these methods, the force constants can be deduced from the induced forces via the Hellman-Feynman theorem[39] when a small displacement on an atom in an otherwise perfect supercell is made. The possibility to calculate exact phonon frequencies at commensurate  $\mathbf{q}$  vectors using smaller non-diagonal unit cells[40] paves the way for very practical applications of these methods. The second approach is based on the density-functional perturbation theory.[41, 42] In this approach, the methods are very versatile because small unit cells

\* ganck@ihpc.a-star.edu.sg

rather than huge supercells are required. Very accurate energy derivatives could be analytically calculated within a computer code[43, 44]. Both approaches could be used together to complement each other[45] for the extraction of higher-order interatomic interactions.[46]

A somewhat simple and effective implementation of a small displacement method is to use a few pre-selected directions in the fractional coordinates that are to be acted upon by appropriate space group operations to deduce the displacement directions as long as the volume  $V$  spanned by the actual displacement directions is nonzero. This strategy may have been inspired by the fact that space group operations[47] usually act on the positions of atoms in fractional coordinates within a unit cell. However, as we shall show later, such implementation may result in a nonoptimal choice of the displacements of atoms that affects the accuracy of the force constants and eventually the lattice dynamical properties. We use a generic orthorhombic system of space group  $Pnma$  with lattice parameters  $a$ ,  $b$ , and  $c$  to show that the volume  $V$  may deviate from its ideal value of 1 and scale unfavorably as  $2(a/b)^{-1} \rightarrow 0$  as  $a \gg b$ . In the case of simulating a graphene sheet using a supercell method, it is shown that a large vacuum thickness could reduce the ideal  $V = 1$  to a value that scales as  $(c/a)^{-2}$  where  $c$  is the vacuum height and  $a$  the hexagonal lattice parameter for graphene. In this paper we propose a displacement method that can be applied to any crystal, encompassing the entire 32 crystallographic point groups and 230 space groups. The displacement directions are deduced directly in the Cartesian coordinates rather than fractional coordinates that are designed to maintain (i) the theoretical maximum for the triple product  $V$  spanned by the three displacements to avoid possible severe roundoff errors, and (ii) a minimal set of irreducible atomic displacements for independent force calculations. To achieve these aims we rely on the concepts of the star of  $k$  and the group of  $k$ [48], defined originally in the reciprocal space but extended to real space in this paper. Various test systems such as Si, graphene, and orthorhombic  $Sb_2S_3$  are used to illustrate the method. This paper is organized as follows. In Section II we provide the full details of our displacement method to make judicious atomic displacements for all crystal symmetries. Section III presents an error analysis for the force constants. Results are shown in Section IV. Finally we conclude in Section V. Appendix A illustrates more clearly how  $V$  may scale poorly with the lattice parameters or the choice of oblique unit cell for a few selected cases.

## II. METHODOLOGY

First we define a matrix

$$A = [\mathbf{a}_1 | \mathbf{a}_2 | \mathbf{a}_3] \quad (1)$$

where the  $i$ th column of  $A$  is taken from the basic lattice translation vector  $\mathbf{a}_i$  of a crystal. For simplicity we use  $A$  to describe a primitive cell but it could be easily extended to deal with a conventional unit cell or even a nonconventional unit cell. A space group operator  $\{R|\mathbf{t}\}$  (in the Seitz notation) corresponds to a rotation matrix

$$R_c = A^{-1}RA \quad (2)$$

in the Cartesian coordinates, which is restricted to either  $p$  or  $\bar{p}$  for  $p = 1, 2, 3, 4$ , and  $6$ .  $p$  means a  $p$ -fold rotation in the international notation, while  $\bar{p}$  means an improper rotation (i.e., a  $p$ -fold rotation followed by an inversion). The 230 space groups are built on top of the 32 crystallographic point groups (see e.g., Refs. [48 and 49]).

In the small displacement method[50] for a phonon calculation of a crystal, if the intrinsic symmetries of a space group are not utilized, we have to sequentially displace all  $N_1$  atoms in a primitive cell embedded in a large  $n_1 \times n_2 \times n_3$  supercell of  $n_1 n_2 n_3 N_1$  atoms along the  $x$ ,  $y$ , and  $z$  Cartesian axes in both positive and negative directions, resulting in  $6N_1$  different supercells, each with one atom displaced slightly compared to the unperturbed supercell (we call this the all-displacement method). Each of the  $6N_1$  supercells will be treated independently where the induced forces are to be calculated so that the interatomic force constants can be deduced. Due to a computational cubic scaling with respect to the number of atoms, most density-functional theory (DFT) implementations[51, 52] face a severe practical issue to handle  $6N_1$  supercells to evaluate the induced forces. It is therefore important to reduce the number of calculations as much as possible.

We now review how the force constant matrix  $\Psi_{ij}$  between the  $i$ th atom in the primitive cell and the  $j$ th atom in the supercell may be calculated. This is achieved by sequentially displacing the  $i$ th atom in the primitive cell by three displacement vectors  $\lambda \mathbf{d}_k^i$  in the Cartesian coordinates,  $k = 1, 2, 3$ , where  $\mathbf{d}_k^i$  is a unit vector.  $\lambda$  is the magnitude of the displacement which is typically  $0.010 \sim 0.015$  Å. For each displacement vector  $\lambda \mathbf{d}_k^i$ , we calculate the induced forces on all atoms in the supercell, in particular the induced force  $\mathbf{F}_k^j$  on the  $j$ th atom,  $k = 1, 2, 3$ . If we make  $\mathbf{F}_k^j$  to constitute the  $k$ th column of a matrix  $F^j$  where

$$F^j = [\mathbf{F}_1^j | \mathbf{F}_2^j | \mathbf{F}_3^j] \quad (3)$$

and similarly we let  $\mathbf{d}_k^i$  to constitute the  $k$ th column of a displacement matrix  $d^i$  where

$$d^i = [\mathbf{d}_1^i | \mathbf{d}_2^i | \mathbf{d}_3^i] \quad (4)$$

then the required force constant  $\Phi_{ij}$  can be calculated from

$$F^j = \lambda \Phi_{ij} d^i \quad (5)$$

From Eq. 5 we see that the displacement vectors  $\mathbf{d}_k^i$  do not need to point along the conventional Cartesian axes but in any directions as long as  $\mathbf{d}^i$  is not singular.

A first level of a possible reduction of the number of calculations can be made if an inequivalent atom in the primitive cell, where its position is commonly known as the Wyckoff position, could be mapped under space group operations to its equivalent atoms in the primitive cell, resulting in a ‘star of  $k$ ’, which is understood to be a set of atoms. We note that the concept of the star of  $k$  is originally defined in the reciprocal space[48]. When handling ‘a star of  $k$ ’, we may arbitrarily choose any atom in a set to be a representative atom (the so-called inequivalent atom) for the purpose of generating the rest of equivalent atoms in the same set. The  $3 \times 3$  force constant matrix  $\Phi_{ij}$  between the  $i$ th inequivalent atom in the primitive cell and another  $j$ th atom in the supercell can be “copied” out[50] to another  $3 \times 3$  force constant matrix  $\Phi_{i'j'}$  between the  $i'$ th equivalent atom and the  $j'$ th atom using

$$\Phi_{i'j'} = R_c \Phi_{ij} R_c^T \quad (6)$$

$R_c$  is as defined in Eq. 2 and  $\{R|\mathbf{t}\}$  maps the  $i$ th atom to the  $i'$ th atom, and the  $j$ th atom to the  $j'$ th atom.  $R_c^T$  is the matrix transpose of  $R_c$ . With this strategy alone (we call this the 6-displacement method), if there are  $N_0$  inequivalent atoms in a primitive cell, then only  $6N_0$  calculations are needed.

However, it may still be possible to reduce the 6 calculations for each of  $N_0$  inequivalent atoms using the site symmetry[49] of an inequivalent atom. The site symmetry (this has the equivalent concept of the group of  $k$ , see for example Ref. [53]) of an inequivalent atom is one of the 32 crystallographic point groups that leaves the position of an inequivalent atom invariant in periodic sense. Note that two different inequivalent atoms from two different stars of  $k$  may not have the same site symmetries.

Now we shall discuss how the site symmetry can be used to reduce the number of displacements for an inequivalent atom. Suppose a displacement  $\mathbf{d}_1^i$  has been applied to an inequivalent  $i$ th atom and the forces on all atoms in the supercell have been found. If an element  $\{R|\mathbf{t}\}$  in the site symmetry of the  $i$ th atom is applied to the supercell with the  $i$ th atom that has been displaced by  $\mathbf{d}_1^i$ , then the net effect of the operation is to rotate the original displacement  $\mathbf{d}_1^i$  to become a displacement  $\mathbf{d}_2^i = R_c \mathbf{d}_1^i$  on the  $i$ th atom. The operation  $\{R|\mathbf{t}\}$  also reshuffles the positions of all atoms in the supercell, as well as to rotate the induced forces caused by  $\mathbf{d}_1^i$  on all atoms in the supercell. This crucial observation implies that without doing an independent (probably expensive) induced force calculation due to  $\mathbf{d}_2^i$ , we are able to just use the information due to  $\mathbf{d}_1^i$  to give us all force information for a virtual  $\mathbf{d}_2^i$  displacement. If there is yet another operation  $\{R|\mathbf{t}\}$  that could rotate  $\mathbf{d}_1^i$  to  $\mathbf{d}_3^i$ , then again an independent displacement of  $\mathbf{d}_3^i$  does not need to be carried out. However, in the case when there is

no extra operation in a site symmetry that can generate an independent  $\mathbf{d}_2^i$  or  $\mathbf{d}_3^i$ , then we have no choice but to carry out necessary separate displacements and find the induced forces to fill up the necessary force field for the  $\Phi_{ij}$  calculation.

In an elegant implementation, the displacement in the Cartesian coordinates  $\mathbf{d}_k^i$  can be generated from the directions defined in the fractional coordinates  $\mathbf{g}_k^i$  where  $\mathbf{d}_k^i = \frac{A\mathbf{g}_k^i}{|A\mathbf{g}_k^i|}$ .  $\mathbf{g}_k^i$  may be chosen from a set of  $S$  that consists of *nonzero* vectors of the form  $(e_1, e_2, e_3)^T$ , where  $e_n = 0, \pm 1$  for  $n = 1, 2, 3$  for simplicity. By systematically applying the elements of the site symmetry to vectors in  $S$ , one may find a minimal set  $S_i$  that contains between one to three vectors.  $S_i$  will generate three  $\mathbf{g}_k^i$  that form a nonzero determinant for  $\mathbf{d}^i$ . This implementation has a slight drawback that may be illustrated by two similar orthorhombic systems  $\text{Bi}_2\text{S}_3$ [54] and  $\text{Sb}_2\text{S}_3$ [6, 19, 50] in the  $Pnma$  setting, where  $a \sim 11.3$  Å,  $b \sim 3.8$  Å, and  $c \sim 11.1$  Å. Here  $a$  is about three times larger than  $b$ . There are twenty atoms in the primitive cell, with five inequivalent atoms on the  $4c$  Wyckoff site. The site symmetry is a group of mirror reflection (a two-element group). The reflection operator  $\bar{2}$  reflects the system across the  $xz$  plane and maps a direction in the fractional coordinate  $\mathbf{g}_1^i = (1, -1, 0)^T$  to  $\mathbf{g}_2^i = (1, 1, 0)^T$ . However, these two directions in the fractional coordinates correspond to  $(a, -b, 0)^T$  and  $(a, b, 0)^T$  in the Cartesian coordinates which subtend an angle not equal to an ideal angle of  $90^\circ$  since  $a \neq b$ . The angle between the two displacements in the Cartesian coordinates is actually given by  $2 \tan^{-1} \frac{b}{a}$  (see Appendix A for a detailed discussion). Hence if  $a$  is much larger than  $b$ , the two vectors  $\mathbf{d}_1^i$  and  $\mathbf{d}_2^i$  are nearly parallel to each other in the Cartesian coordinates. However the operation is a physical reflection in the  $xz$  plane and hence it is possible to force the angle between the two displaced vectors to be exactly  $90^\circ$ , thereby achieving the largest determinant for  $\mathbf{d}^i$  of 1 for matrix inversion in Eq. 5.

In another example, a graphene sheet of a lattice constant  $a$  and a vacuum thickness  $c$  may use  $\mathbf{g}_1^i = (1, 0, 1)^T$  to generate  $\mathbf{g}_2^i = (0, 1, -1)^T$  and  $\mathbf{g}_3^i = (-1, -1, 1)^T$  with the point group operations. This means only one independent force calculation is to be performed. However, an analysis shows that  $V = \det \mathbf{d}^i = \frac{a^2 c \sqrt{3}}{2(a^2 + c^2)^{3/2}}$ , which goes to  $\frac{\sqrt{3}/2}{(c/a)^2}$  for a large  $c/a$  ratio. With[55]  $c = 20$  Å and  $a = 2.471$  Å,  $V = 0.013$ . However, with the method to be developed later, we find that the angles between any two displacements taken from  $\mathbf{d}_k^i$ ,  $k = 1, 2, 3$  can be made  $90^\circ$  thereby making  $V$  achieves its largest value of 1.

To develop a sense of how the inaccuracy of forces and  $V = \det \mathbf{d}^i$  may affect the accuracy of force constants, we consider the force constants in the  $xy$  plane for the  $4c$  site of the  $Pnma$  space group. Here  $\mathbf{d}_1^i = \frac{1}{\sqrt{a^2 + b^2}}(a, -b)^T$

and  $\mathbf{d}_2^i = \frac{1}{\sqrt{a^2+b^2}}(a, b)^T$ . From Eq. 5, we have

$$[\mathbf{F}_1^j | \mathbf{F}_2^j] = \lambda [\Phi_{ij}^1 | \Phi_{ij}^2] \frac{1}{\sqrt{a^2+b^2}} \begin{pmatrix} a & a \\ -b & b \end{pmatrix} \quad (7)$$

We then have

$$\Phi_{ij}^2 = \frac{1}{2\lambda} \left( \frac{a^2}{b^2} + 1 \right)^{\frac{1}{2}} (\mathbf{F}_2^j - \mathbf{F}_1^j) \quad (8)$$

If  $a \gg b$ , then  $\mathbf{d}_1^i$  and  $\mathbf{d}_2^i$  are almost parallel to each other resulting in very similar forces  $\mathbf{F}_1^j$  and  $\mathbf{F}_2^j$ . If the force  $\mathbf{F}_1^j$  due to  $\mathbf{d}_1^i$  is not determined accurately enough,  $\mathbf{F}_2^j$  will inherit the same inaccuracy since it is ‘copied’ from  $\mathbf{F}_1^j$  through a symmetry operation, then  $\Phi_{ij}^2$  will be inaccurate due to a large roundoff error that is amplified by a large geometry factor  $\left( \frac{a^2}{b^2} + 1 \right)^{\frac{1}{2}}$ .

Now we present a method that will systematically deduce the displacement directions directly in the *Cartesian coordinates* for a forward difference scheme with the aim of maintaining a largest possible magnitude for the determinant of  $d^i$  and a minimum number of independent displacements. The displacement method must also maintain the minimal number of independent displacements when a central difference scheme is used for an improved accuracy for  $\Phi_{ij}$ . For a central difference scheme, we need to displace the atoms in  $-\mathbf{d}_k^i$ ,  $k = 1, 2, 3$  where  $\mathbf{d}_k^i$  have been chosen for a forward difference scheme. We note that two operations are able to map  $\mathbf{d}_k^i$  to  $-\mathbf{d}_k^i$ : one is the inversion operator, and the other a 2-fold rotation.

The task may at first seem arduous for all 32 crystallographic point groups (see Table I). However, there are actually four distinct cases to consider.[56] The first case deals with the triclinic crystals and covers point groups 1 to 2 ( $C_1$  and  $C_i$ ) that involve a single 1 or  $\bar{1}$  operation. The second case handles the monoclinic crystals and covers point groups 3 to 5 ( $C_2$ ,  $C_s$ ,  $C_{2h}$ ) that involve a single 2 or  $\bar{2}$  operation. The third case deals with the orthorhombic crystals and covers point groups 6 to 8 ( $D_2$ ,  $C_{2v}$ ,  $D_{2h}$ ). These point groups possess three operations involving either 2 or  $\bar{2}$  that are perpendicular to one another. Finally the fourth case deals with the remaining four crystal systems, i.e., tetragonal, trigonal, hexagonal, and cubic crystals and covers point groups 9 to 32. These point groups have a single 3,  $\bar{3}$ , 4, or  $\bar{4}$  operation.

Usually, the principal axis (the axis with the highest symmetry) is not pointing along the  $z$  axis but along a vector  $\mathbf{n}$  characterized by the polar angle  $\theta$  and azimuthal angle  $\phi$ . To ease the discussion of the determination of  $\mathbf{d}_k^i$ , we transform all operations  $R_c$  to  $R'_c$  in the site symmetry according to  $R'_c = Q^{-1}R_cQ$ ,  $Q = R_z(\phi)R_y(\theta)$ . Here  $R_y(\theta)$  [ $R_z(\phi)$ ] is a rotation of angle  $\theta$  ( $\phi$ ) around the  $y$  ( $z$ ) axis. Under such transformation, the operation with the principal axis  $R_{\mathbf{n}}(\eta)$  will be mapped to  $R_z(\eta)$  where the rotation axis is now along the  $z$  axis. This can be easily seen since  $R_{\mathbf{n}}(\eta)$  is transformed to  $R_z(\eta)$  via

Crystal	Symmetry	$n_{\text{FD}}$	$n_{\text{CD}}$
Triclinic	$C_1$	3	6
	$C_i$	3	3
Monoclinic	$C_2$	2	3
	$C_s$	2	4
	$C_{2h}$	2	2
Orthorhombic	$D_2$	1	2
	$C_{2v}$	1	2
	$D_{2h}$	1	1
Tetragonal	$C_4$	1	2
	$S_4$	1	2
	$C_{4h}$	1	1
	$D_4$	1	1
	$C_{4v}$	1	2
	$D_{2d}$	1	1
	$D_{4h}$	1	1
Trigonal	$C_3$	1	2
	$S_6$	1	1
	$D_3$	1	1
	$C_{3v}$	1	2
	$D_{3d}$	1	1
Hexagonal	$C_6$	1	2
	$C_{3h}$	1	2
	$C_{6h}$	1	1
	$D_6$	1	1
	$C_{6v}$	1	2
	$D_{3h}$	1	1
	$D_{6h}$	1	1
Cubic	$T$	1	1
	$T_h$	1	1
	$O$	1	1
	$T_d$	1	1
	$O_h$	1	1

TABLE I.  $n_{\text{CD}}$  ( $n_{\text{FD}}$ ) is the minimal number of displacements per atom for a central (forward) difference scheme.

$R_z(\eta) = Q^{-1}R_{\mathbf{n}}(\eta)Q$  or  $R_{\mathbf{n}}(\eta) = QR_z(\eta)Q^{-1}$ . Once we find  $\mathbf{d}'^i_k$  in the rotated frame, we obtain  $\mathbf{d}^i_k = Q\mathbf{d}'^i_k$ .

### A. The first case

First we consider the triclinic cell where there are two point groups  $C_1(1)$  and  $C_i(\bar{1})$ . For  $C_1(1)$  the symmetry is so low that we simply propose to displace the  $i$ th atom in  $x+$ ,  $y+$ , and  $z+$ , resulting in three independent displacements for a forward difference scheme. In this case,  $V = \det d^i$  attains its largest possible value of unity. For a central difference scheme, we need to displace the atom

in  $x-$ ,  $y-$ , and  $z-$ , resulting a total of six displacements. For  $C_i(1)$ , an inversion operator exists that could map  $\mathbf{d}_k^i$  to  $-\mathbf{d}_k^i$  hence we need to do the same number of displacements (i.e., 3) for both the forward and central difference schemes (see the third row of Table I).

### B. The second case

For the monoclinic cell there are three point groups to consider. We first consider  $C_2(2)$ , we propose to use a first displacement  $\mathbf{d}_1^i = (0, -1, 1)^T$ . Under a 2-fold rotation around the  $z$  axis, we generate a second displacement  $\mathbf{d}_2^i = (0, 1, 1)^T$  from  $\mathbf{d}_1^i$ . We exhaust all operations in this point group, hence we propose a second independent displacement vector  $\mathbf{d}_3^i = (1, 0, 0)^T$ . This choice makes  $V$  to attain its largest possible value of unity. For a central difference scheme, we need to displace the  $i$ th atom in  $-\mathbf{d}_1^i$  independently since there is no operation in the site symmetry that is able to map  $\mathbf{d}_1^i$  to its negative. However, the 2-fold rotation is able to map  $\mathbf{d}_3^i = (1, 0, 0)^T$  to its negative  $(-1, 0, 0)^T$ . Hence the total number of displacements is three for the point group  $C_2(2)$  instead of four for a central difference scheme. For the second point group  $C_s(m)$ . There is no operation that can map  $\mathbf{d}_1^i$  and  $\mathbf{d}_3^i$  to their negatives. Hence the number of independent displacements is four for a central difference scheme. The third point group to consider is  $C_{2h}$ . Since there is an inversion operator the number of displacements for the forward and central difference schemes are the same, which is two.

### C. The third case

For the next three point groups for the orthorhombic cells  $D_2(222)$ ,  $C_{2v}(mm2)$ , and  $D_{2h}(mmm)$ , we simply need to displace an atom in  $\mathbf{d}_1^i = \frac{1}{\sqrt{3}}(1, 1, 1)$  direction. This direction is obtained by maximizing a test vector  $(t, u, v)^T$  and its images  $(t, -u, -v)$  (under a 2-fold rotation around the  $x$ -axis) and  $(-t, u, -v)$  (under a 2-fold rotation around the  $y$ -axis) thus forming a triple product of  $V = 4tuv$ . The magnitude of the displacement vector is constrained according to  $t^2 + u^2 + v^2 = 1$ . A standard Lagrange multiplier method gives a possible solution  $\mathbf{d}_1^i = \frac{1}{\sqrt{3}}(1, 1, 1)^T$  that delivers the largest  $V = \frac{4}{\sqrt{27}} = 0.7698$ .

For  $D_2$  and  $C_{2v}$  there is no operation that could map  $\mathbf{d}_1^i$  to  $-\mathbf{d}_1^i$  hence we need to do a total of two displacements for a central difference scheme. However,  $D_{2h}$  has an inversion operator that results in the same number (i.e., one) of independent displacement for both the forward and central difference schemes.

### D. The fourth case

For the next 24 point groups from  $C_4(4)$  to  $O_h(m\bar{3}m)$  covering tetragonal, trigonal, hexagonal, and cubic cells, we note that we have either 3 or  $\bar{3}$  or 4 or  $\bar{4}$  that is able to generate  $\mathbf{d}_2^i$  and  $\mathbf{d}_3^i$  from just one  $\mathbf{d}_1^i$ . For these point groups, using the Lagrange multiplier method, we find that a single displacement is able to give a maximum  $V$  of  $\frac{4}{\sqrt{27}}$  and 1 for  $C_4$  and  $C_3$ , respectively, with a test vector of  $\mathbf{d}_1^i = (t, u, \frac{1}{\sqrt{3}})^T$ ,  $t^2 + u^2 = \frac{2}{3}$ . In order to prepare  $\mathbf{d}_1^i$  to be mapped under an existing  $C_2$  operation (which is unfortunately missing in eight point groups  $C_4$ ,  $S_4$ ,  $C_{4v}$ ,  $C_3$ ,  $C_{3v}$ ,  $C_6$ ,  $C_{3h}$ , and  $C_{6v}$ ) to  $-\mathbf{d}_1^i$  with the  $C_2$  rotation axis pointing along  $(n_x, n_y, n_z)$  direction, we can find the values of  $t$  and  $u$  by solving the simultaneous equations  $t^2 + u^2 = \frac{2}{3}$  and  $n_x t + n_y u + \frac{n_z}{\sqrt{3}} = 0$ . This is equivalent to solving a quadratic equation  $(n_x^2 + n_y^2)u^2 + \frac{2}{\sqrt{3}}n_y n_z u + \frac{1}{3}(n_z^2 - 2n_x^2) = 0$ . To see more clearly the nature of solutions to the quadratic equation, without loss of generality we assume the axis of rotation for  $C_2$  is in the  $yz$  plane making an angle  $\theta$  with the  $z$  axis where  $(n_x, n_y, n_z) = (0, \sin \theta, \cos \theta)$ . This gives two solutions  $(t, u, v) = (\pm \sqrt{1 - \frac{1}{3\sin^2 \theta}}, -\frac{\cos \theta}{\sqrt{3}\sin \theta}, \sqrt{\frac{1}{3}})$ . For  $\theta = \frac{\pi}{2}$ ,  $(t, u, v) = (\pm \sqrt{\frac{2}{3}}, 0, \sqrt{\frac{1}{3}})$ . As  $\theta$  is decreased from  $\frac{\pi}{2}$ , two solutions will approach one another along the circumference of a circle and coincide with one another when  $\theta$  becomes a critical angle  $\theta_c = \sin^{-1} \sqrt{\frac{1}{3}} = 35.26^\circ$  and the solution is  $(t, u, v) = (0, -\sqrt{\frac{2}{3}}, \sqrt{\frac{1}{3}})$ . When  $\theta < \theta_c$ , there is no real solution.

## III. ERROR ANALYSIS FOR THE FORCE CONSTANTS

Now we perform a detailed error analysis for the displacement method. We shall focus on  $\Phi_{ij}$  which is the  $3 \times 3$  force constant matrix block between the  $i$ th atom and the  $j$ th atom based on Eq. 5. Since atom pairs are now understood, we suppress the index  $i$  in  $\mathbf{d}^i$  and index  $j$  in  $F^j$  for forces in Eq. 5. We let the exact force  $\mathbf{F}_k$  to differ from the approximate force  $\mathbf{f}_k$  by an error term  $\lambda \epsilon_k$  that measures the intrinsic inaccuracies where

$$\mathbf{f}_k = \mathbf{F}_k + \lambda \epsilon_k, \quad k = 1, 2, 3 \quad (9)$$

The calculated force constant block with  $d$  is given by

$$\begin{aligned} \Phi_d &= [\mathbf{f}_1 | \mathbf{f}_2 | \mathbf{f}_3](\lambda d)^{-1} \\ &= F(\lambda d)^{-1} + [\epsilon_1 | \epsilon_2 | \epsilon_3]d^{-1} \\ &= \Phi_e + \epsilon d^{-1} \end{aligned} \quad (10)$$

where  $\Phi_e$  is the exact force constant matrix and  $\epsilon = [\epsilon_1 | \epsilon_2 | \epsilon_3]$ . Eq. 10 clearly shows that the error can be attributed by the intrinsic inaccuracy of the force and the inverse of  $d$ , which could potentially be large if  $d$  is

near singular. In the absence of the exact force constant  $\Phi_e$  to calculate errors we rely on

$$\phi_d - \phi_{d_0} = \epsilon(d^{-1} - d_0^{-1}) \quad (11)$$

where  $d_0$  is chosen to be with the largest possible  $V$ . We will study the inaccuracy of the calculated force constant as a function of  $V$  in the next section.

#### IV. RESULTS

To confirm the methodology outline above, we carry out density-functional theory (DFT) calculations within the local density approximation, with projector augmented-wave (PAW) pseudopotential as implemented in the Vienna Ab initio Simulation Package (VASP) [57] on a generic system of silicon. We use a 2-atom primitive rhombohedral cell and a  $3 \times 3 \times 3$  supercell for the phonon calculations. The cutoff energy for the plane-wave basis set is 307 eV. We use a  $3 \times 3 \times 3$   $k$  mesh for the supercell calculations. The magnitude of the displacement  $\lambda$  is 0.015 Å. Because of the presence of a  $C_3$  rotation with its rotation axis along the  $(1, 1, 1)^T$  direction in the Cartesian coordinates and another  $C_2$  operation in Si just one displacement is sufficient for a central difference scheme for the phonon calculations. However, since we want to study the effect of  $V$  on the phonon dispersions, we will still utilize  $C_3$  in the  $(1, 1, 1)^T$  direction to rotate  $\mathbf{d}_1 = (x, y, y)^T$  that results in just one displacement if the forward difference scheme is used. However another displacement in the negative direction is needed for a central difference scheme since the  $C_2$  operation is now no longer able to map  $\mathbf{d}_1$  to  $-\mathbf{d}_1$ . Under  $C_3$  with its rotation axis in  $(1, 1, 1)^T$ , we have  $\mathbf{d}_2 = (y, x, y)$ , and  $\mathbf{d}_3 = (y, y, x)$ . This gives  $V = x^3 - 3xy^2 + 2y^3$ . With the constraint on the magnitude of  $\mathbf{d}_1$ , which gives  $2x^2 + y^2 = 1$ , we solve for  $x$  and  $y$  using a Newton-Raphson scheme for a predetermined  $V$ . We notice that  $V \rightarrow 0$  as  $x$  and  $y$  go to  $\frac{1}{\sqrt{3}}$ .

We investigate the error of the force constants as measured by the Frobenius norm  $\|\phi_d - \phi_{d_0}\|_F$  as a function  $V$  using Eq. 11. We use  $\det d_0 = 1$ . Fig. 1 shows the error of the force constants linearly increases with decreasing  $V = \det d$ .

For an estimate of  $\epsilon$  in Eq. 11 without a full knowledge of the error of the induced forces, we proceed by assuming  $\epsilon = \epsilon_0 J$ , which is characterized by a single error parameter  $\epsilon_0$  and an appropriate  $J$  matrix. Our aim is to estimate  $\epsilon_0$  that measures the inaccuracy of the force by fitting the RHS of Eq. 11. We observe that in the limit when  $V$  is very small, the three displacement vectors  $\mathbf{d}_1$ ,  $\mathbf{d}_2$ , and  $\mathbf{d}_3$  become closer and closer to another and converge to  $\frac{1}{\sqrt{3}}(1, 1, 1)^T$ . To maximize error it is therefore reasonable to assume  $\epsilon_1 = \epsilon_0(1, -1, -1)^T$ ,  $\epsilon_2 = \epsilon_0(-1, 1, -1)^T$ , and  $\epsilon_3 = \epsilon_0(-1, -1, 1)^T$ . Under such assumption and with Eq 11 we obtain a rather good fit and deduce  $\epsilon_0 = 3.7 \times 10^{-4}$  eV/Å<sup>2</sup>. This in

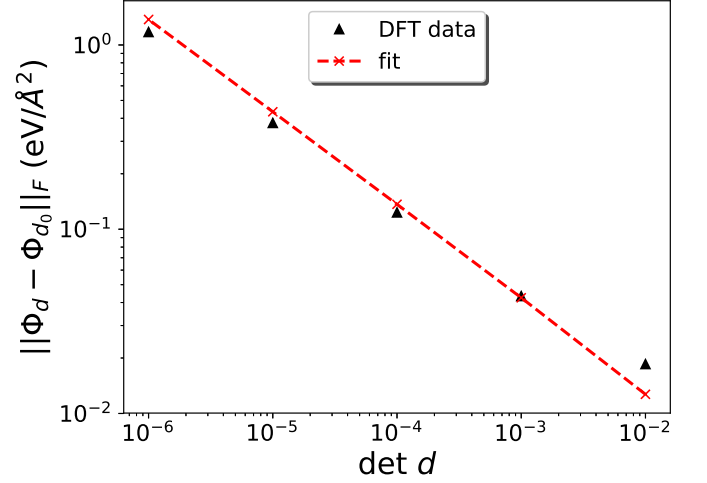


FIG. 1. The error (filled triangle) characterized by the Frobenius norm of the force constant block  $\phi_d - \phi_{d_0}$  in Eq. 11 as a function  $V = \det d$ . The fitting form according to the RHS of Eq. 11 gives  $\epsilon_0 = 3.7 \times 10^{-4}$  eV/Å<sup>2</sup>.

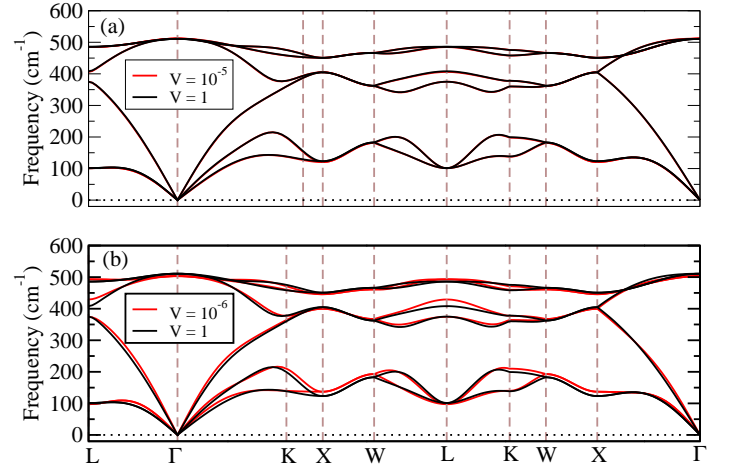


FIG. 2. (a) The comparison of phonon dispersions obtained with  $V = 10^{-5}$  and  $V = 1$ . (b) The comparison of phonon dispersions obtained with  $V = 10^{-6}$  and  $V = 1$ .

turn gives a reasonable estimate of the force inaccuracy of  $\lambda\epsilon_0 = 5.6 \times 10^{-6}$  eV/Å. Fig. 2 shows phonon dispersions with different  $V$  values. Noticeable differences in phonon dispersions are observed when  $V$  reaches  $10^{-6}$ .

We select four representative systems to perform more phonon calculations. For each system, we first carry out a phonon calculation by using the symmetry-adapted atomic displacements. Using identical computational parameters (i.e., energy cutoff,  $k$  mesh, etc), we carry out a second phonon calculation by displacing each inequivalent atom in the  $x+$ ,  $x-$ ,  $y+$ ,  $y-$ ,  $z+$ , and  $z-$  along the Cartesian axes. The results for hexagonal MoS<sub>2</sub> [space group (SG) # 194], trigonal Bi<sub>2</sub>Se<sub>3</sub> (SG # 166), orthorhombic Sb<sub>2</sub>S<sub>3</sub> (SG # 62), and a 2D graphene sheet

	symmetry- adapted	6- displacement	all- displacement
MoS <sub>2</sub>	3	12	36
Bi <sub>2</sub> Se <sub>3</sub>	5	18	30
Sb <sub>2</sub> S <sub>3</sub>	20	30	120
Graphene	1	6	12

TABLE II. The numbers of atomic displacements required for the symmetry-adapted, 6-displacement, and all-displacement methods. The numbers of displacements for 6-displacement and all-displacement methods are  $6n_{\text{ineq}}$  and  $6n_c$ , respectively. Here  $n_{\text{ineq}}$  is the number of inequivalent atoms in the unit cell and  $n_c$  is the number of atoms in the unit cell.

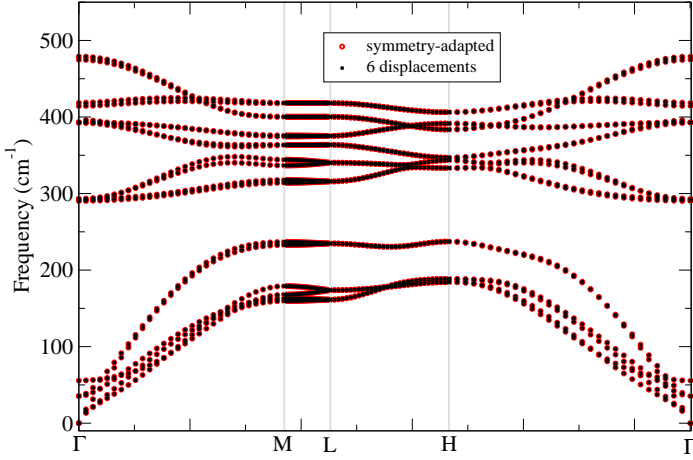


FIG. 3. Phonon dispersions of hexagonal MoS<sub>2</sub> with  $a = 3.123$  and  $c = 12.087$  Å obtained with (a) symmetry-adapted atomic displacements and (b) six displacements for each of the two inequivalent atoms. The effect of longitudinal optical (LO) and transverse optical (TO) splitting[50] has been taken account. A  $3 \times 3 \times 2$  supercell is used. The cutoff energy for the plane-wave basis set is 700 eV. A  $k$  mesh of  $2 \times 2 \times 1$  is used for electronic relaxation. The selected  $\mathbf{q}$  points (in  $\mathbf{b}_1$ ,  $\mathbf{b}_2$ , and  $\mathbf{b}_3$ ) are  $\Gamma = [0, 0, 0]$ ,  $M = [0, \frac{1}{2}, 0]$ ,  $L = [0, \frac{1}{2}, \frac{1}{2}]$ , and  $H = [\frac{1}{3}, \frac{1}{3}, \frac{1}{2}]$ .

(SG # 191) are shown in Figs. 3, 4, 5, and 6, respectively. For all calculations the local density approximation is used, and the magnitude of the displacement  $\lambda$  is 0.015 Å. It is seen that the phonon dispersions obtained with both displacement methods are essentially the same that indicate a correct implementation of the proposed methodology. The efficacy of the symmetry-adapted atomic displacement method is shown in Table II.

## V. CONCLUSION

In summary, we have proposed a systematic displacement method that guarantees a theoretical optimal vol-

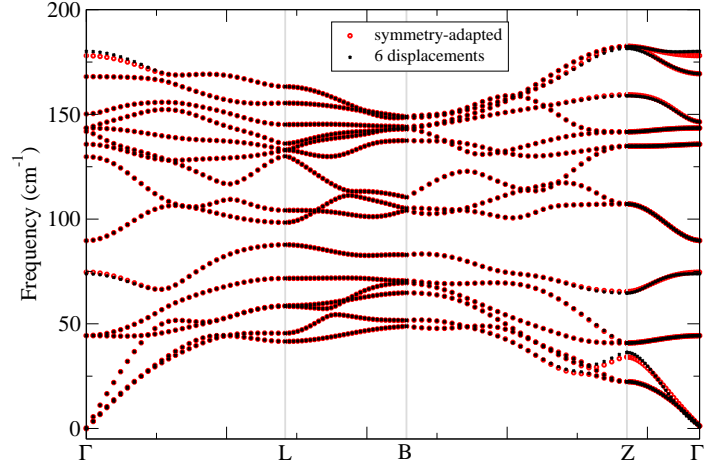


FIG. 4. Phonon dispersions of trigonal Bi<sub>2</sub>Se<sub>3</sub> with  $a_r = 9.621$  Å,  $\alpha_r = 24.64^\circ$ , which corresponds to a conventional hexagonal cell of  $a = 4.105$  and  $c = 27.973$  Å, obtained with (a) symmetry-adapted atomic displacements and (b) six displacements for each of the three inequivalent atoms. The effect of longitudinal optical (LO) and transverse optical (TO) splitting[50] has been taken account. The supercell is  $4 \times 4 \times 1$  of the conventional hexagonal unit cell. The cutoff energy for the plane-wave basis set is 423.2 eV. A  $k$  mesh of  $4 \times 4 \times 2$  is used for electronic relaxation. The selected  $\mathbf{q}$  points (in  $\mathbf{b}_1$ ,  $\mathbf{b}_2$ , and  $\mathbf{b}_3$ ) are  $\Gamma = [0, 0, 0]$ ,  $L = [\frac{1}{2}, 0, 0]$ ,  $B = [\eta, \frac{1}{2}, 1 - \eta]$ , and  $Z = [\frac{1}{2}, \frac{1}{2}, \frac{1}{2}]$ , where  $\eta = (1 + 4 \cos \alpha_r)/(2 + 4 \cos \alpha_r)$ . [58]

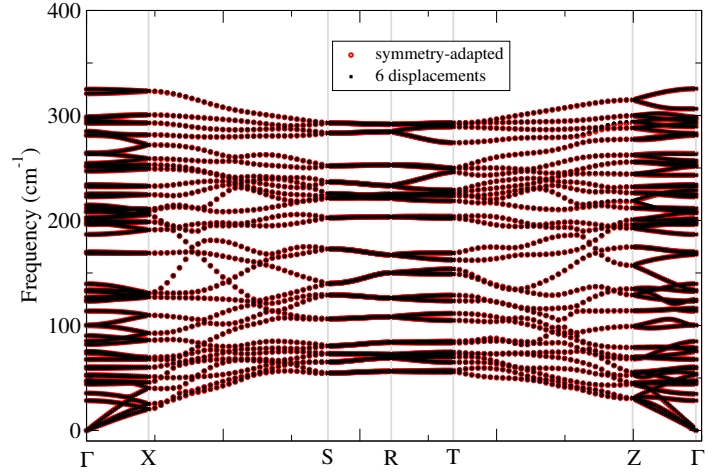


FIG. 5. Phonon dispersions of orthorhombic Sb<sub>2</sub>S<sub>3</sub> with  $a = 11.011$ ,  $b = 3.812$ , and  $c = 10.794$  Å obtained with (a) symmetry-adapted atomic displacements and (b) six displacements for each of the five inequivalent atoms. The effect of longitudinal optical (LO) and transverse optical (TO) splitting[50] has been taken account. A  $2 \times 4 \times 2$  supercell is used. The cutoff energy for the plane-wave basis set is 323.3 eV. A  $k$  mesh of  $2 \times 3 \times 2$  is used for electronic relaxation. The selected  $\mathbf{q}$  points (in  $\mathbf{b}_1$ ,  $\mathbf{b}_2$ , and  $\mathbf{b}_3$ ) are  $\Gamma = [0, 0, 0]$ ,  $X = [\frac{1}{2}, 0, 0]$ ,  $S = [\frac{1}{2}, \frac{1}{2}, 0]$ ,  $R = [\frac{1}{2}, \frac{1}{2}, \frac{1}{2}]$ ,  $T = [0, \frac{1}{2}, \frac{1}{2}]$ , and  $Z = [0, 0, \frac{1}{2}]$ .



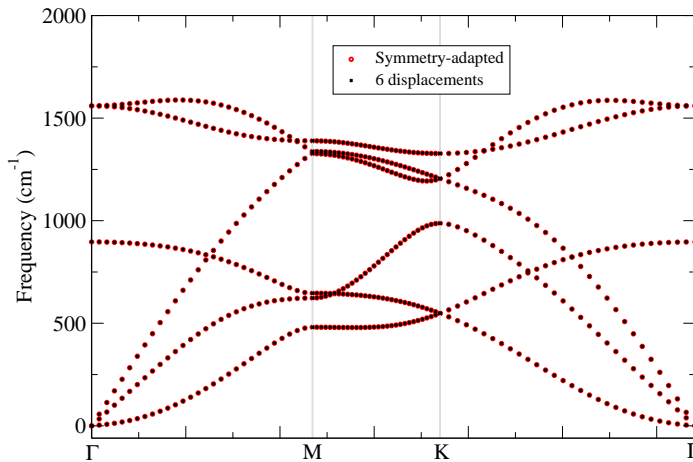


FIG. 6. Phonon dispersions of 2D graphene sheet with  $a = 2.462 \text{ \AA}$  and a vacuum height of  $12 \text{ \AA}$  obtained with (a) a symmetry-adapted atomic displacement and (b) six displacements for the only inequivalent atom. A  $4 \times 4 \times 1$  supercell is used. The cutoff energy for the plane-wave basis set is  $500 \text{ eV}$ . A  $k$  mesh of  $6 \times 6 \times 1$  is used for electronic relaxation. The selected  $\mathbf{q}$  points (in  $\mathbf{b}_1$ ,  $\mathbf{b}_2$ , and  $\mathbf{b}_3$ ) are  $\Gamma = [0, 0, 0]$ ,  $M = [0, \frac{1}{2}, 0]$ , and  $K = [\frac{1}{3}, \frac{1}{3}, 0]$ .

ume  $V$  spanned by the displacement vectors to minimize possible severe roundoff errors for lattice dynamical studies. The concepts of the star of  $k$  and the group of  $k$  that are originally defined in the reciprocal space have been extended to real space to facilitate a practical implemen-

tation of the method that is readily applied to all 32 crystallographic point groups and all 230 space groups. The method generates a minimal set of irreducible displacement vectors to keep the number of independent force calculations to a minimum. The error in the calculated force constants is shown to explicitly depend on the inverse of the volume  $V$  spanned by the displacement directions and the intrinsic accuracy in the induced forces. This justified the use of the Cartesian coordinates rather than the fractional coordinates to optimize  $V$ . Several test systems have been used to illustrate the method. The method is shown to be very effective in dealing cells with a large aspect ratio due to a huge difference in lattice parameters, cells with a large vacuum separation, and cells that are very oblique due to an unconventional choice of a primitive cell. We expect the strategies employed in this paper could be extended to deal with higher order interatomic interactions for efficiency and accuracy.

## VI. ACKNOWLEDGMENT

We acknowledge fruitful discussions with J. F. Kong. We thank the National Supercomputing Center, Singapore (NSCC) and A\*STAR Computational Resource Center, Singapore (ACRC) for computing resources. This work is supported by RIE2020 Advanced Manufacturing and Engineering (AME) Programmatic Grant No A1898b0043.

- 
- [1] M. Born and K. Huang, *Dynamical Theory of Crystal Lattices* (Oxford University Press, London, 1956).
  - [2] A. van de Walle and G. Ceder, The effect of lattice vibrations on substitutional alloy thermodynamics, *Rev. Mod. Phys.* **74**, 11 (2002).
  - [3] C. K. Gan, X. F. Fan, and J.-L. Kuo, Composition-temperature phase diagram of  $\text{Be}_x\text{Zn}_{1-x}\text{O}$  from first principles, *Comput. Mater. Sci.* **49**, S29 (2010).
  - [4] W. Zhong, R. D. King-Smith, and D. Vanderbilt, Giant LO-TO splittings in perovskite ferroelectrics, *Phys. Rev. Lett.* **72**, 3618 (1994).
  - [5] Y. Zhao, X. Luo, H. Li, J. Zhang, P. T. Araujo, C. K. Gan, J. Wu, H. Zhang, S. Y. Quek, M. S. Dresselhaus, and Q. H. Xiong, Interlayer breathing and shear modes in few-trilayer  $\text{MoS}_2$  and  $\text{WSe}_2$ , *Nano Lett.* **13**, 1007 (2013).
  - [6] W. K. Chong, G. Xing, Y. Liu, E. L. Gui, Q. Zhang, Q. Xiong, N. Mathews, C. K. Gan, and T. C. Sum, Direct measurement of coherent phonon dynamics in solution-processed stibnite thin films, *Phys. Rev. B* **90**, 035208 (2014).
  - [7] D. Giovanni, W. K. Chong, Y. Y. F. Liu, H. A. Dewi, T. Yin, Y. Lekina, Z. X. Shen, N. Mathews, C. K. Gan, and T. C. Sum, Coherent spin and quasiparticle dynamics in solution-processed layered 2D lead halide perovskites, *Adv. Sci.* **5**, 1800664 (2018).
  - [8] F. Giustino, Electron-phonon interactions from first-principles, *Rev. Mod. Phys.* **89**, 015003 (2017).
  - [9] A. Togo, F. Oba, and I. Tanaka, First-principles calculations of the ferroelastic transition between rutile-type and  $\text{CaCl}_2$ -type  $\text{SiO}_2$  at high pressures, *Phys. Rev. B* **78**, 134106 (2008).
  - [10] G. Grimvall, *Thermophysical Properties of Materials* (Elsevier Science B.V., Amsterdam, The Netherlands, 1999).
  - [11] A. Mujica, A. Rubio, A. Munoz, and R. J. Needs, High-pressure phases of group-IV, III-V, and II-VI compounds, *Rev. Mod. Phys.* **75**, 863 (2003).
  - [12] N. Mounet and N. Marzari, First-principles determination of the structural, vibrational and thermodynamic properties of diamond, graphite, and derivatives, *Phys. Rev. B* **71**, 205214 (2005).
  - [13] P. B. Allen, Theory of thermal expansion: Quasi-harmonic approximation and corrections from quasiparticle renormalization, *Mod. Phys. Lett. B* **34**, 2050025 (2020).
  - [14] C. Malica and A. D. Corso, Quasi-harmonic temperature dependent elastic constants: Applications to silicon, aluminum, and silver, *J. Phys.: Condens. Matter* **32**, 315902 (2020).
  - [15] C. Toher, J. J. Plata, O. Levy, M. de Jong, M. Asta, M. BuongiornoNardelli, and S. Curtarolo, High-throughput computational screening of thermal conduc-



- tivity, Debye temperature, and Grüneisen parameter using a quasiharmonic Debye model, *Phys. Rev. B* **90**, 174107 (2014).
- [16] G. J. Snyder and E. S. Toberer, Complex thermoelectric materials, *Nature Mater.* **7**, 105 (2008).
- [17] G. K. H. Madsen, A. Katre, and C. Bera, Calculating the thermal conductivity of the silicon clathrates using the quasi-harmonic approximation, *Phys. Stat. Sol. (A)* **213**, 802 (2016).
- [18] P. Gorai, V. Stevanović, and E. Toberer, Computationally guided discovery of thermoelectric materials, *Nature Rev. Mat.* **2**, 17053 (2017).
- [19] C. K. Gan, J. R. Soh, and Y. Liu, Large anharmonic effect and thermal expansion anisotropy of metal chalcogenides: The case of antimony sulfide, *Phys. Rev. B* **92**, 235202 (2015).
- [20] B. Arnaud, S. Lebègue, and G. Raffy, Anisotropic thermal expansion of bismuth from first principles, *Phys. Rev. B* **93**, 094106 (2016).
- [21] C. K. Gan and Y. Y. F. Liu, Direct calculation of the linear thermal expansion coefficients of MoS<sub>2</sub> via symmetry-preserving deformations, *Phys. Rev. B* **94**, 134303 (2016).
- [22] C. P. Romao, Anisotropic thermal expansion in flexible materials, *Phys. Rev. B* **96**, 134113 (2017).
- [23] C. K. Gan and C. H. Lee, Anharmonic phonon effects on linear thermal expansion of trigonal bismuth selenide and antimony telluride crystals, *Comput. Mater. Sci.* **151**, 49 (2018).
- [24] C. K. Gan and K. T. E. Chua, Large thermal anisotropy in monoclinic niobium trisulfide: A thermal expansion tensor study, *J. Phys.: Condens. Matter* **31**, 265401 (2019).
- [25] C. H. Lee and C. K. Gan, Anharmonic interatomic force constants and thermal conductivity from Grüneisen parameters: An application to graphene, *Phys. Rev. B* **96**, 035105 (2017).
- [26] G. Petretto, S. Dwaraknath, H. P. Miranda, D. Winston, M. Giantomassi, M. J. van Setten, X. Gonze, K. A. Persson, G. Hautier, and G.-M. Rignanese, Data descriptor: High-throughput density-functional perturbation theory phonons for inorganic materials, *Scientific Data* **5**, 180065 (2018).
- [27] A. Togo, Phonon database at Kyoto University, <http://phonondb.mtl.kyoto-u.ac.jp> (2020).
- [28] S. Curtarolo, G. L. W. Hart, M. BuongiornoNardelli, N. Mingo, S. Sanvito, and O. Levy, The high-throughput highway to computational materials design, *Nature Mater.* **12**, 191 (2013).
- [29] S. P. Ong, W. D. Richards, A. Jain, G. Hautier, M. Kocher, S. Cholia, D. Gunter, V. L. Chevrier, K. A. Persson, and G. Ceder, Python materials genomics (pymatgen): A robust, open-source python library for material analysis, *Comput. Mater. Sci.* **68**, 314 (2013).
- [30] G. Pizzi, A. Cepellotti, R. Sabatini, N. Marzari, and B. Kozinsky, Aiida: automated interactive infrastructure and database for computational science, *Comput. Mater. Sci.* **111**, 218 (2016).
- [31] K. Parlinski, Z. Q. Li, and Y. Kawazoe, First-principles determination of the soft mode in cubic ZrO<sub>2</sub>, *Phys. Rev. Lett.* **78**, 4063 (1997).
- [32] Y. Wang, L.-Q. Chen, and Z.-K. Liu, YPHON: A package for calculating phonons of polar materials, *Comput. Phys. Comm.* **185**, 2950 (2014).
- [33] Y. Wang, S.-L. Shang, H. Fang, Z.-K. Liu, and L.-Q. Chen, First-principles calculations of lattice dynamics and thermal properties of polar solids, *npj Comp. Mater.* **2**, 16006 (2016).
- [34] G. J. Ackland, M. C. Warren, and S. J. Clark, Practical methods in ab initio lattice dynamics, *J. Phys.: Condens. Matter* **9**, 7861 (1997).
- [35] A. Togo and I. Tanaka, First principles phonon calculations in materials science, *Scr. Mater.* **108**, 1 (2015).
- [36] A. Togo, Phonopy, <https://phonopy.github.io/phonopy> (2020).
- [37] D. Alfè, Phon: A program to calculate phonons using the small displacement method, *Comput. Phys. Comm.* **180**, 2622 (2009).
- [38] G. Kresse, J. Furthmüller, and J. Hafner, Ab initio force constant approach to phonon dispersion relations of diamond and graphite, *Europhys. Lett.* **32**, 729 (1995).
- [39] R. P. Feynman, Forces in molecules, *Phys. Rev.* **56**, 340 (1939).
- [40] J. H. Lloyd-Williams and B. Monserrat, Lattice dynamics and electron-phonon coupling calculations using non-diagonal supercells, *Phys. Rev. B* **92**, 184301 (2015).
- [41] S. Baroni, S. de Gironcoli, A. Dal Corso, and P. Giannozzi, Phonons and related crystal properties from density-functional perturbation theory, *Rev. Mod. Phys.* **73**, 515 (2001).
- [42] X. Gonze, First-principles responses of solids to atomic displacements and homogeneous electric fields: Implementation of a conjugate-gradient algorithm, *Phys. Rev. B* **55**, 10337 (1997).
- [43] P. Giannozzi, S. Baroni, N. Bonini, M. Calandra, R. Car, C. Cavazzoni, D. Ceresoli, G. L. Chiarotti, M. Cococcioni, I. Dabo, A. Dal Corso, S. de Gironcoli, S. Fabris, G. Fratesi, R. Gebauer, U. Gerstmann, C. Gougoussis, A. Kokalj, M. Lazzeri, L. Martin-Samos, N. Marzari, F. Mauri, R. Mazzarello, S. Paolini, A. Pasquarello, L. Paulatto, C. Sbraccia, S. Scandolo, G. Sclauzero, A. P. Seitsonen, A. Smogunov, P. Umari, and R. M. Wentzcovitch, Quantum Espresso: a modular and open-source software project for quantum simulations of materials, *J. Phys.: Condens. Matter* **21**, 395502 (2009).
- [44] X. Gonze, B. Amadon, P.-M. Anglade, J.-M. Beuken, F. Bottin, P. Boulanger, F. Bruneval, D. Caliste, R. Caracas, M. Cote, T. Deutsch, L. Genovese, P. Ghosez, M. Giantomassi, S. Goedecker, D. Hamann, P. Hermet, F. Jollet, G. Jomard, S. Leroux, M. Mancini, S. Mazevet, M. Oliveira, G. Onidab, Y. Pouillon, T. Rangel, G.-M. Rignanese, D. Sangalli, R. Shaltaf, M. Torrent, M. Verstraete, G. Zerah, and J. Zwanziger, ABINIT: First-principles approach to material and nanosystem properties, *Comput. Phys. Comm.* **180**, 2582 (2009).
- [45] L. Fu, M. Kornbluth, Z. Cheng, and C. A. Marianetti, Group theoretical approach to computing phonons and their interactions, *Phys. Rev. B* **100**, 014303 (2019).
- [46] K. Parlinski, Ab initio determination of anharmonic phonon peaks, *Phys. Rev. B* **98**, 054305 (2018).
- [47] T. Hahn(Ed.), *International Tables for Crystallography (2006). Vol. A, Space-group symmetry* (Chester, International Union of Crystallography, 2006).
- [48] M. S. Dresselhaus, G. Dresselhaus, and A. Jorio, *Group theory: Application to the physics of condensed matter* (Springer-Verlag, Berlin, Heidelberg, 2008).
- [49] G. Burns, *Solid State Physics* (Academic Press, Orlando, Florida, 1985).

- [50] Y. Liu, K. T. E. Chua, T. C. Sum, and C. K. Gan, First-principles study of the lattice dynamics of  $\text{Sb}_2\text{S}_3$ , *Phys. Chem. Chem. Phys.* **16**, 345 (2014).
- [51] M. C. Payne, M. P. Teter, D. C. Allan, T. A. Arias, and J. D. Joannopoulos, Iterative minimization techniques for ab initio total-energy calculations: molecular dynamics and conjugate gradients, *Rev. Mod. Phys.* **64**, 1045 (1992).
- [52] C. K. Gan, P. D. Haynes, and M. C. Payne, Preconditioned conjugate gradient method for the sparse generalized eigenvalue problem in electronic structure calculations, *Comput. Phys. Comm.* **134**, 33 (2001).
- [53] S. L. Altmann, *Band theory of solids: An introduction from the point of view of symmetry* (Oxford University Press, Walton Street, Oxford OX2 6DP, 1991).
- [54] Y. Y. Zhao, K. T. E. Chua, C. K. Gan, J. Zhang, B. Peng, Z. P. Peng, and Q. H. Xiong, Phonons in  $\text{Bi}_2\text{S}_3$  nanostructures: Raman scattering and first-principles studies, *Phys. Rev. B* **84**, 205330 (2011).
- [55] C. K. Gan and D. J. Srolovitz, First-principles study of graphene edge properties and flake shapes, *Phys. Rev. B* **81**, 125445 (2010).
- [56] See an implementation of our algorithm in fm-forces.f90 from <https://github.com/qphonon/atomic-displacement>.
- [57] G. Kresse and J. Furthmüller, Efficiency of ab-initio total energy calculations for metals and semiconductors using a plane-wave basis set, *Comput. Mater. Sci.* **6**, 15 (1996).
- [58] W. Setyawan and S. Curtarolo, High-throughput electronic band structure calculations: Challenges and tools, *Comput. Mater. Sci.* **49**, 299 (2010).
- [59] M. Nespolo and M. I. Aroyo, The crystallographic chameleon: when space groups change skin, *Acta Cryst. A* **72**, 523 (2016).

## Appendix A: Investigation of the determinant of $d$

We consider a generic example of  $\text{Sb}_2\text{S}_3$  crystal with space group of  $Pnma$  (SG # 62) which has an orthorhombic cell. We shall investigate the determinant of  $d$  (see Eq. 4) as a function of cell dimensions  $a$ ,  $b$ , and  $c$ . For a general discussion we choose a primitive cell with  $\mathbf{a}_1 = a\mathbf{i} + nb\mathbf{j}$ ,  $\mathbf{a}_2 = b\mathbf{j}$ , and  $\mathbf{a}_3 = c\mathbf{k}$ , where  $n$  is an integer.  $\mathbf{i}$ ,  $\mathbf{j}$ , and  $\mathbf{k}$  are unit vectors in the Cartesian directions. First we consider  $n = 0$  that corresponds to the conventional primitive cell.

For  $\text{Sb}_2\text{S}_3$  crystal, all five inequivalent atoms occupy the 4c Wyckoff position hence we may just consider any one of them. The site symmetry for the 4c position consists of just two elements:

$$I = \begin{pmatrix} 1 & 0 & 0 \\ 0 & 1 & 0 \\ 0 & 0 & 1 \end{pmatrix} \quad (\text{A1})$$

and

$$m = \begin{pmatrix} 1 & 0 & 0 \\ 0 & -1 & 0 \\ 0 & 0 & 1 \end{pmatrix} \quad (\text{A2})$$

which is a reflection across the  $xz$  plane.

$\mathbf{g}_1$  may be chosen to be  $(1, -1, 0)^T$  which will be mapped to  $\mathbf{g}_2 = (1, 1, 0)^T$  under  $m$ . A second independent displacement is  $\mathbf{g}_3 = (0, 0, 1)^T$ .

As discussed in the main text, the actual displacement in the Cartesian coordinates is  $\mathbf{d}_k^i = \lambda \frac{A\mathbf{g}_k}{|A\mathbf{g}_k|}$ ,  $k = 1, 2, 3$ . We find

$$V = \det d \quad (\text{A3})$$

$$= \frac{\det A}{|A\mathbf{g}_1||A\mathbf{g}_2||A\mathbf{g}_3|} \quad (\text{A4})$$

$$= \frac{2ab}{\sqrt{a^2 + (n-1)^2b^2}\sqrt{a^2 + (n+1)^2b^2}} \quad (\text{A5})$$

while the angle  $\theta$  between the displacements  $\mathbf{d}_1^i$  and  $\mathbf{d}_2^i$  satisfies

$$\cos \theta = \frac{a^2 + (n^2 - 1)b^2}{\sqrt{a^2 + (n-1)^2b^2}\sqrt{a^2 + (n+1)^2b^2}} \quad (\text{A6})$$

When  $n = 0$ , we find  $V = \frac{2ab}{a^2+b^2}$  (therefore  $V \rightarrow 2(a/b)^{-1}$  for  $a \gg b$ ) and  $\cos \theta = \frac{a^2-b^2}{a^2+b^2}$ . The last result is equivalent to a simpler expression of  $\tan^{-1} \frac{\theta}{2} = \frac{b}{a}$ , consistent with the fact that the two displacements are  $(a, -b, 0)^T$  and  $(a, b, 0)^T$  in the Cartesian coordinates. If  $a$  is much larger than  $b$ , then  $V$  decreases as  $\frac{2b}{a}$  to zero while  $\cos \theta$  approaches 1 since the two displacements  $\mathbf{d}_1^i$  and  $\mathbf{d}_2^i$  are almost parallel.

Next we discuss the effect of  $n \neq 0$ . The site symmetry operations become[59]

$$I = \begin{pmatrix} 1 & 0 & 0 \\ 0 & 1 & 0 \\ 0 & 0 & 1 \end{pmatrix} \quad (\text{A7})$$

and

$$m = \begin{pmatrix} 1 & 0 & 0 \\ -2n & -1 & 0 \\ 0 & 0 & 1 \end{pmatrix} \quad (\text{A8})$$

If  $\mathbf{g}_1 = (1, 0, 0)^T$  is used, the  $m$  operation on  $\mathbf{g}_1$  gives  $\mathbf{g}_2 = (1, -2n, 0)^T$ . A second independent displacement is  $\mathbf{g}_3 = (0, 0, 1)^T$ . For a simple analysis, we set  $a = b$ . For large  $n$ , we find  $V$  approaches  $-\frac{2}{n}$ , while  $\cos \theta$  approaches  $-1$ , which means the displacement  $\mathbf{d}_1^i$  approaches  $-\mathbf{d}_2^i$ .

This shows that using displacement directions in the form of nonzero  $(e_1, e_2, e_3)^T$  where  $e_i = 0, \pm 1$ ,  $i = 1, 2, 3$  may not be an optimal choice.